

Ru–C–ZnO Composite Catalysts for the Synthesis of Methyl Isobutyl Ketone via Single Step Gas Phase Acetone Self-Condensation

Abdulaziz A. Bagabas · Mohamed Mokhtar ·
Vagif M. Akhmedov · Katabathini Narasimharao ·
Sulaiman N. Basahel · Abdulrahman Al-Rabiah

Received: 16 January 2014 / Accepted: 29 March 2014
© Springer Science+Business Media New York 2014

Abstract Ruthenium/activated charcoal (Ru–C) was modified by a solid–solid interaction method with synthesized *nano*-zinc oxide (*n*-ZnO). Three different ratios of Ru–C:*n*-ZnO (1:2, 1:1 and 3:2) were used to prepare Ru–C–ZnO composite catalysts. These were used in the gas-phase, one-step self-condensation of acetone to methyl isobutyl ketone (MIBK). The composite catalyst (1:1 ratio) contained 2.5 wt% Ru showed superior conversion of acetone and selectivity for MIBK. Furthermore, this catalyst showed good consistency for MIBK formation for 100 h without any deactivation. Characterization of the catalysts revealed that balanced hydrogenation and acid–base functional character is crucial to obtain high catalytic performance.

Keywords Ruthenium-activated charcoal · Nano-ZnO · Acidic/basic site concentration ratio · Ru-loading · Acetone self-condensation · Methyl isobutyl ketone

A. A. Bagabas (✉)
Petrochemicals and Refining Center, Petrochemicals Research
Institute, King Abdulaziz City for Science and Technology,
P.O. Box 6086, Riyadh 11442, Kingdom of Saudi Arabia
e-mail: abagabas@hotmail.com

M. Mokhtar · K. Narasimharao · S. N. Basahel
Department of Chemistry, Faculty of Science, King Abdulaziz
University, P.O. Box 80203, Jeddah 21589, Kingdom of Saudi
Arabia

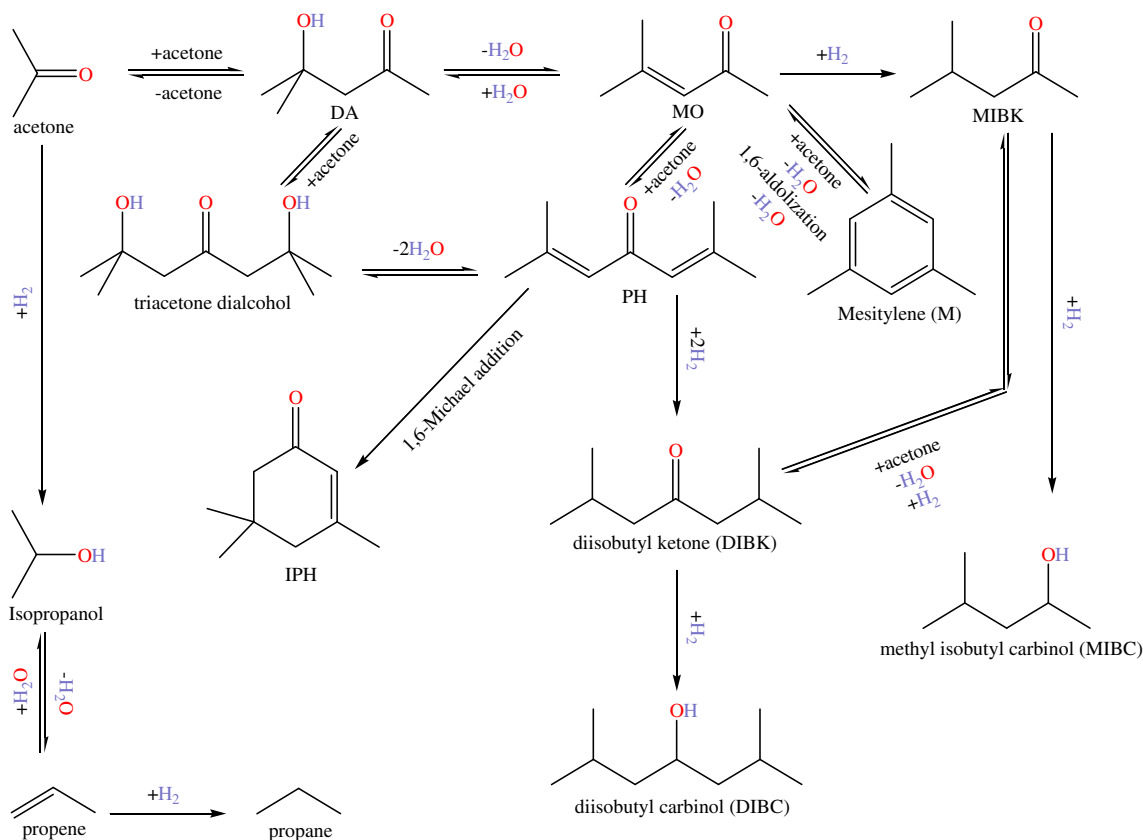
V. M. Akhmedov
Department of Chemistry, Baku State University, Zahid Xalilov
St. 23, Baku, Azerbaijan Republic

A. Al-Rabiah
Department of Chemical Engineering, College of Engineering,
King Saud University, Riyadh 11451, Kingdom of Saudi Arabia

1 Introduction

The conversion of inexpensive organic compounds, such as acetone, to high-value chemicals is highly relevant for industrial applications [1, 2]. One example of such a chemical is methyl isobutyl ketone (MIBK), which is widely used in a number of applications including: in paints, as a liquid–liquid extraction solvent, as a solvent for vinyl, epoxy and acrylic resin production, for the removal of paraffin from mineral oils, in the synthesis of rubber chemicals, and in fine chemistry applications [3, 4]. The global demand for MIBK is estimated to be 300,000 tons per year. Historically, MIBK was produced via a three-step, homogeneous catalytic process from acetone [5] (Scheme 1). The first step is the self-condensation of acetone to diacetone alcohol (DA), the second step is the dehydration of DA to mesityl oxide (MO) and the final step is the selective hydrogenation of the carbon–carbon double bond of MO to form MIBK. This process thus involves several unit operations, resulting in high capital and operating costs and inherent inefficiencies. Some unwanted side reactions also occur; the most commonly observed are over-condensation and non-selective hydrogenations. Consequently, it is desirable to produce MIBK from acetone in a single stage and a number of catalytic systems have been proposed that aim to reduce the number of steps and side reactions.

A significant study has investigated the use of supported transition metals to catalyze the condensation of acetone (dimethylketone, DMK) to α,β -unsaturated ketone, followed by another in situ catalytic reduction step. It has been reported that MIBK can be produced from acetone and hydrogen in one step in a catalytic distillation reactor [6].



Scheme 1 Reaction pathway of conventional process for the production of MIBK

Bi-functional catalysts, such as Pd- or Pt-supported on sulfonated resins, which have condensation, dehydration and hydrogenation capabilities, are used for this reaction [7], which is undertaken under high pressures and thus adds significant cost to the overall procedure. The MIBK also needs to be extracted from the effluent in the reactor and purified, as its concentration is usually lower than 30 wt%. It is, therefore, of great interest to develop novel catalysts, which can offer comparable or better MIBK yields at lower temperatures and under atmospheric pressure. Ideally, the catalyst should be versatile so that it can be used in the production of a variety of aliphatic low molecular weight ketones.

Talwalkar and Mahajani [8] summarized the conversion rates and selectivities of the most promising catalysts reported to date for MIBK synthesis from acetone. Group VIII or IB metals, such as Pd, Pt, Ni and Cu, on acidic or basic supports such as zeolites, mixed transition metal oxides and ion exchange resins, have been extensively investigated. Most notably, Pd [9–11] and Ni [12, 13] supported on Mg–Al or Zn–Cr mixed oxides, alumina, H-ZSM-5, Cu/MgO [14], Cu–Mg alloy powders [15] and Pd–Zr–P multifunctional Pd-polyoxometalate catalytic system [16] are reported to catalyze this process

in the gas-phase at ambient pressure. A Pd/CuO/Al₂O₃/SiO₂ catalyst offered 30 % acetone conversion with 60 % MIBK selectivity at 230 °C under atmospheric pressure. Several studies have also been focused on the application of different supports with acid–base surface functionality; metal catalysts supported on activated carbon (C) provided high activity and selectivity for MIBK from acetone [17]. Recently, we reported the addition of *n*-ZnO to Pd metal catalysts and how the composition of metal and *n*-ZnO is influencing the activity and selectivity of acetone condensation reaction [18]. It was determined that 1.0 wt% Pd supported on *n*-ZnO and 1.0 wt% Pd supported on a *n*-ZnO and CrO₃ composite material were highly active and selective catalysts for a one-step, gas-phase synthesis of MIBK from acetone at atmospheric pressure. To achieve better MIBK selectivity in the self-condensation of acetone, it seems that the catalyst should possess basic sites of medium strength along with hydrogenation activity [9]. It is known that Ru–C is an effective hydrogenation catalyst [19] and ZnO possesses both acidic and basic sites [20]. To develop a catalyst which possesses hydrogenation and acid–base properties, we chose to prepare a composite of Ru–C and *n*-ZnO.

In this study, we have investigated the one-step gas-phase self-condensation process of acetone using *n*-ZnO as the substrate, which possesses both acid and base properties. Our working hypothesis is that activated charcoal, with its characteristically high surface area, can enhance the dispersion of ZnO nanoparticles. Moreover, it is anticipated that the hydrophobicity of this charcoal can hinder the interaction between the active sites and water molecules. The results reported here indicate that the combination of Ru, ZnO, and activated charcoal (Ru–C–ZnO) creates a unique catalyst system for the gas-phase condensation reaction. To investigate the interactions of the three components in the Ru–C–ZnO catalysts, several characterization techniques (XRD, TEM, N₂-adsorption, chemisorption and TPD/TPR) were utilized. We also studied the effect of reaction temperature, concentration of acid–base sites and Ru-loading on catalytic performance. To best of our knowledge, the application of Ru–C–ZnO composite catalysts for the aforementioned reaction has not previously been reported.

2 Experimental

2.1 Chemicals

Acetone (Winlab HPLC grade, 99.8 %), hydrogen gas (99.9 %), sodium pyruvate (Sigma-Aldrich, ≥99 %), hydroxylamine hydrochloride (Carlo-Erba, 99 %), sodium hydrogen carbonate (Fluka, ≥99.5 %), zinc sulfate heptahydrate (BDH, 99.5 %), and ruthenium 5 wt% on activated charcoal catalyst (Ru–C, Winlab) were purchased and were used without further purification.

2.2 Preparation of Catalysts

n-ZnO was prepared following the procedure reported by Bagabas et al. [21]. An appropriate amount of aqueous solution of ZnSO₄·7H₂O was combined with an aqueous solution of sodium pyruvic acid oxime monohydrate [Na(PAO)H₂O], which was prepared from sodium pyruvate, hydroxylamine hydrochloride, and sodium hydrogen carbonate in aqueous medium. The white precipitate of Zn(PAO)₂(H₂O)₂ was filtered off, then dried under vacuum overnight, and subsequently calcined for approximately 12 h at 400 °C in a muffle furnace to obtain pure *n*-ZnO.

A solid–solid interaction method was adopted to synthesize the composite of Ru–C–ZnO catalysts. Ru/AC and *n*-ZnO in different ratios were mixed thoroughly using a pestle and mortar then the mixture was pulverized at room temperature using a pulverizing machine and subsequently the composites were calcined at 400 °C for 12 h. The ratios of Ru–C:*n*-ZnO used were as follows: 1:2 wt% (CAT-II),

1:1 wt% (CAT-III) and 3:2 wt% (CAT-IV). For comparison, the pure *n*-ZnO (CAT-I) and pure Ru–C (CAT-V) catalysts were also studied.

2.3 Characterization of Catalysts

The phase identification for the calcined catalysts were performed using a Philips ‘X’ pert pro’ diffractometer, operated at 40 kV and 40 mA, using CuK_α radiation, in the 2θ range from 2° to 100° in steps of 0.02°, with a sampling time of 1 s/step. The average crystallite size was calculated using Scherrer’s equation:

$$D_{hkl} = K\lambda / (B_{hkl} \cos \theta) \quad (1)$$

where D_{hkl} is the average crystallite size of the phase under investigation, K is the Scherrer’s constant (0.89), λ is the wavelength of the X-ray beam used (1.54056 Å), B_{hkl} is the full width at half maximum (FWHM) of the analyzed diffraction peak (101) and θ is the diffraction angle.

A Philips CM200FEG microscope, 200 kV, equipped with a field emission gun was used for transmission electron microscopy (TEM) analysis. The coefficient of spherical aberration was $C_s = 1.35$ mm. The information limit was better than 0.18 nm. High-resolution images with a pixel size of 0.044 nm were taken with a CCD camera.

The BET-surface area of the prepared catalysts was estimated from N₂ adsorption at –196 °C using a Quantachrome Autosorb-1-MP instrument. The acidic and basic properties of each catalyst was determined by the temperature-programmed desorption (TPD) technique with ammonia (NH₃) and carbon dioxide (CO₂) respectively, using a TPD/R/O 1100 thermo electron instrument. Typically, calcined sample of 50 mg was first pre-treated in helium gas at 150 °C for 2 h, and then cooled to 30 °C. Subsequently the sample was saturated with NH₃ or CO₂ at this temperature for 1 h. The initial flushing with helium gas was done in order to remove any excess NH₃ or CO₂. The TPD profiles were recorded with a thermal conductivity detector at a heating rate of 283 K min^{–1} from room temperature to 500 °C under a continuous flow of helium gas. Quantachrome CHEMBET 3000 was used to perform the TPR analysis of catalysts. The experiments were carried out using a gas mixture of 5 % H₂ in Ar at a flow rate of 30 mL min^{–1} with a linear heating ramp of 278 K min^{–1} up to 600 °C. The amount of H₂ consumed was monitored as a function of temperature on a thermal conductivity detector (TCD).

The metal surface area and dispersion were determined by H₂ pulse chemisorption experiments using a micro-metrics AutoChem 2910 instrument. Approximately 50 mg of catalyst was treated at 150 °C for 16 h under vacuum prior to starting the experiment. The catalyst was loaded into the sample tube and the sample heated to 400 °C at the

rate of $10\text{ }^{\circ}\text{C min}^{-1}$ under a mixed H_2/Ar (5/95 vol%) gas flow of 10 mL min^{-1} . The sample was kept under these conditions for 1 h, and then it was flushed for 1 h by switching the flow to helium gas. After completion of the reduction process, the temperature of the sample was decreased to $70\text{ }^{\circ}\text{C}$ and pulses of H_2 were initiated to determine the volume of H_2 uptake. The metal surface area and dispersion were determined from the hydrogen consumption by the sample.

2.4 Catalytic Activity Measurements

All catalysts were activated by reducing the catalyst at $400\text{ }^{\circ}\text{C}$ under a H_2 gas flow of 60 mL min^{-1} over night, prior to catalytic testing. The self-condensation of acetone was performed at reaction temperatures of 250 , 300 , 350 and $375\text{ }^{\circ}\text{C}$ respectively, under hydrogen flow, at atmospheric pressure, in a glass tubular fixed-bed micro reactor (ID 0.9 cm). The reactor was placed in a vertical tubular furnace and the catalyst sample ($\sim 250\text{ mg}$) was loaded into the reactor between two layers of pyrex glass wool and pieces of ceramic. The $\text{H}_2/\text{acetone}$ molar ratio was maintained at 1.5, 3, 4.5 or 6. Acetone was introduced to the reactor by a Hitachi HPLC pump (Model L-2100/2130), connected to a heated tube set to $65\text{ }^{\circ}\text{C}$ for its delivery as a vapor mixed with H_2 before entering the reaction zone at the top of the catalyst bed. A K-type thermocouple was placed in the center of the catalyst to monitor the reaction temperature. The liquid products were condensed at $-40\text{ }^{\circ}\text{C}$ and collected every hour, and subsequently analyzed off-line using a Varian CP-3800 gas chromatograph, equipped with a flame ionization detector (FID) and a $50 \times 0.32 \times 1.2\text{ mm}^3$ CP-Wax 58 CB column. The gaseous downstream flow was analyzed online by a refinery gas analyzer Varian CP-3800 GC, equipped with an FID and TCD. The products were identified by GC using standard samples.

3 Results and Discussion

3.1 Powder X-ray Diffraction

The crystalline phases, as well as the average crystallite size of the catalysts, were determined from the powder XRD patterns shown in Fig. 1. The CAT-V sample was shown to have an amorphous nature, whereas CAT-I was highly crystalline as depicted by the diffraction peaks corresponding to the wurtzite phase of ZnO [JCPDS 36-1451]. It is clear that wurtzite is the dominant phase in all the composite catalysts, similar to the pure $n\text{-ZnO}$ sample. The average crystallite size of each of the catalysts was determined using Eq. 1 and the values are shown in

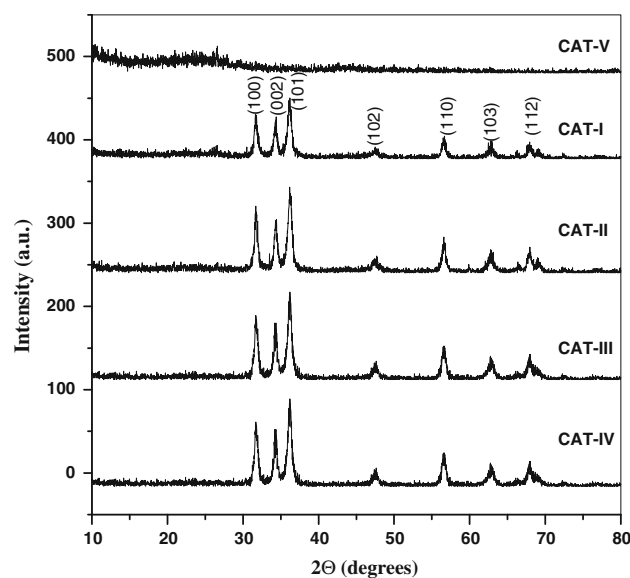


Fig. 1 XRD patterns of all the investigated catalysts

Table 1. In this instance, CAT-I was found to have an average crystallite size of 20 nm. The preparation procedure is known to have great influence on the phase and particle size of ZnO. The typical particle size of nano-sized ZnO varies from 10 to 40 nm. There is a little difference in crystallite size of CAT-II (23 nm) and CAT-I (20 nm). However, a more pronounced change was observed by further increasing the wt% of Ru-C; CAT-III and CAT-IV showed an average crystallite size of 25 and 30 nm respectively.

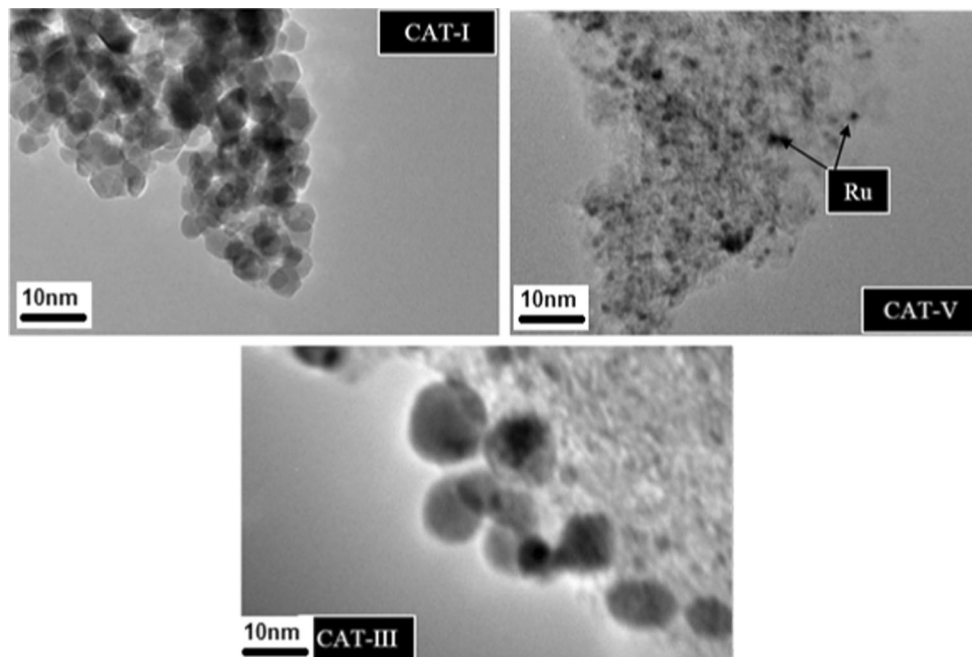
The crystallite size of Ru metal in Ru-C (CAT-V) sample was not determined because of its amorphous nature. Previously, Navale et al. [22] reported structural parameters of crystalline Ru-doped ZnO materials. They observed an increase in the average crystallite size of the materials with the increase in Ru content and pretreatment temperature. An increase of the crystallite size from 16 to 36 nm was observed when the Ru content changed from 1.0 to 3.0 wt%. During the calcination step, there is a clear possibility for oxidation of Ru to ruthenium oxide, however diffraction peaks corresponding to ruthenium oxide were not observed for any of the composite materials probably due to very fine dispersion of those particles.

3.2 TEM Analysis

TEM analysis was performed (Fig. 2) to obtain more detailed information about the average crystallite size and structure of the catalysts. The TEM image for pure $n\text{-ZnO}$ (CAT-I) powder shows hexagonal ZnO crystallites of approximately 3–6 nm in diameter. Whereas, the pure

Table 1 Results from XRD and N₂ adsorption measurements of all the investigated catalysts

Catalyst	Major phase ^a	Crystallite size (nm) ^a	Ru loading (wt%)	S _{BET} (m ² g ⁻¹)	S _{Ru} ^b (m ² g ⁻¹)	Ru dispersion ^b (%)
CAT-I	wurtzite	20	0.0	37	–	–
CAT-II	wurtzite	23	1.67	300	24.36	5.00
CAT-III	wurtzite	25	2.5	289	30.70	6.31
CAT-IV	wurtzite	30	3.0	278	25.73	5.29
CAT-V	amorphous	–	5.0	327	22.43	4.61

^a Powder XRD measurements^b H₂-chemisorption measurements; catalysts were treated at 150 °C for 16 h under vacuum before starting measurements**Fig. 2** TEM images of the representative catalysts

Ru–C sample (CAT-V) showed a sponge-like amorphous structure and black spots, which are observed on the surface of activated charcoal, indicate dispersed Ru nano particles. A TEM image of a selected composite catalyst (CAT-III) can also be seen in the Fig. 2c. It can be concluded from the image analysis of CAT-III that the ZnO crystallite size is not uniform. Furthermore, the amorphous nature of carbon has not changed after *n*-ZnO incorporation.

Navale et al. [22] calculated the average crystallite size using Scherrer's equation and the size is in the range from 20 to 130 nm for Ru–ZnO samples. In our work, we have not observed such a large change in the crystallite size of the calcined composite samples. This difference is thought to be due to the different method of preparation used and that the composite catalysts consist of amorphous C as one of the components.

3.3 N₂ Adsorption–Desorption

BET-surface areas (S_{BET}), calculated from the nitrogen adsorption/desorption isotherms of composite catalysts, are given in Table 1. CAT-I was determined to have a surface area of 37 m² g⁻¹, which is large for a highly crystalline oxide such as ZnO. The micro-crystalline ZnO shows a surface area in the range of 5–10 m² g⁻¹ [23]. Nanometer-sized particles of ZnO have very different physical and chemical properties compared with the bulk material. When used as catalysts, their catalytic activity is expected to be enhanced not only because of their increased surface area, but also because of the changes in surface properties, such as surface defects. The CAT-V sample was found to have a high surface area of 327 m² g⁻¹.

It is known that the textural properties of commercially available Ru–C samples depend upon the manufacturing

process, as well as the nature of the carbon used [15]. The major contribution to the surface area of the Ru–C catalyst results from the surface structure of activated charcoal. The surface areas of the composite catalysts are lower than that of the pure Ru–C, therefore, mixing of Ru–C and *n*-ZnO leads to a decrease in surface area. We compared the surface area of the composite catalysts with theoretical Ru wt% loading (Table 1) and found that the surface area decreases with increasing Ru metal loading. Other composite catalysts showed similar behavior, where a decrease of surface area is observed upon increasing Ru loading. Furthermore, as described in the literature [24], it is possible that agglomerated particles of Ru–ZnO could partially block the pores of active carbon leading to a decrease of its available surface for N₂ adsorption.

3.4 H₂ Chemisorption

The Ru-metallic surface area, as well as its degree of dispersion over the calcined composite catalysts, was determined using H₂ pulse chemisorption at 70 °C (Table 1). Bachiller-Baeza et al. [25], studied the reducibility of mono- and bi-metallic Ru–C catalysts. They observed a two-stage reduction process for both type of catalyst; the first reduction was at a low temperature (~225 °C) and the other at higher temperature (~400 °C). For this reason, we reduced the catalysts at 400 °C to achieve the complete reduction of Ru and ZnO present in the composite materials. The trend of both metallic surface area and the degree of dispersion of Ru metal in all the composite catalysts was similar. An increased Ru loading resulted in an increase of metallic surface area and degree of dispersion, except in the case of the CAT-III sample, for which the apparent maximum values of both metallic surface area and degree of dispersion were obtained. This is thought to be due to an optimum loading effect of *n*-ZnO, which interacts with the Ru metal. The CAT-I sample adsorbed the H₂, but the volume of H₂ uptake is relatively low compared to any of the other composite catalysts. The partial reduction of ZnO at low temperature has been reported in the literature for the bimetallic supported system, Ru–Zn/SiO₂ [26], and the H₂ consumption peaks were assigned to H₂ chemisorption on ZnO (ZnO + H₂ → ZnH–OH). Neri et al. [27] rejected this pathway, and explained that the peak at low temperature could be due to a spill-over mechanism by which hydrogen, dissociatively adsorbed on metallic Ru, migrates to the ZnO support and reduces it, yielding metallic Zn and water.

CAT-IV chemisorbed a higher amount of hydrogen than Ru–C, which clearly indicates that there are more Ru and Zn surface atoms accessible to hydrogen in this composite catalyst. This could be explained by the larger interactive particle size, detected by XRD. The reducibility of surface

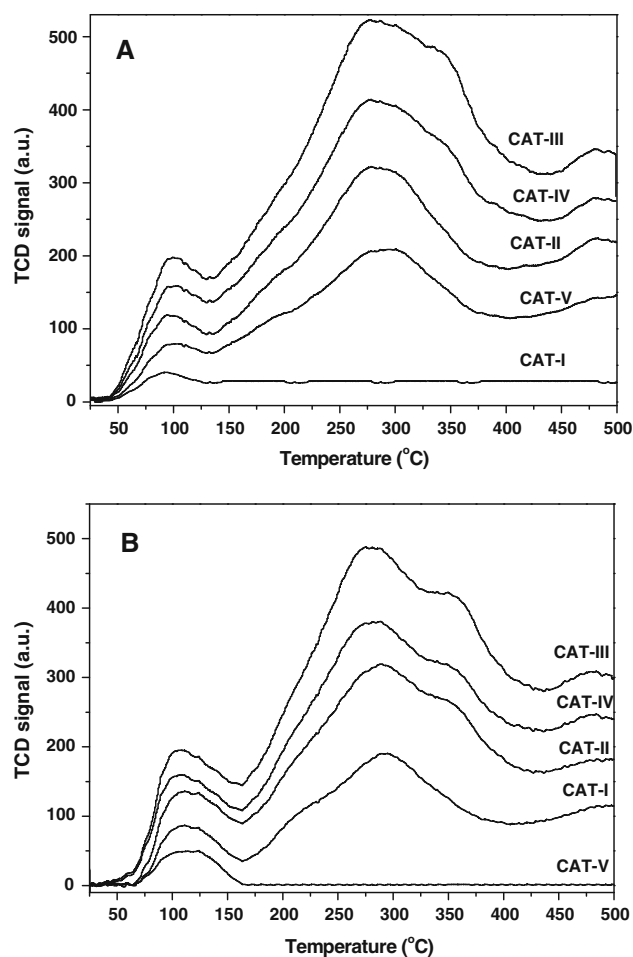


Fig. 3 TPD patterns of all the investigated catalysts **a** NH₃ and **b** CO₂

metal oxides has been described as being affected by the presence of a noble metal and in general the reduction temperature of the oxide becomes lower [25–27]. It has also been reported that heating, in the presence of H₂ gas, induces the formation of alloy phases (thermodynamically favorable) between metallic Zn and active noble metals such as Ru or Pt even at low temperatures [28, 29].

3.5 Acid–Base Properties

The acid–base properties of the calcined catalysts were measured by NH₃ and CO₂-TPD experiments. Figure 3a shows the NH₃-TPD profiles of the *n*-ZnO and composite materials. For the CAT-I sample, a single desorption peak centered at 95 °C can be attributed to the physically adsorbed NH₃ on the surface of *n*-ZnO. In contrast, CAT-V (Ru–C) sample showed two desorption peaks at 100 °C and 290 °C. These two peaks can be attributed to physically adsorbed NH₃ and moderate acid sites, respectively. The CAT-II (33.3 wt% of Ru–C) sample showed a similar desorption pattern as CAT-V. An additional desorption

peak at 340 °C can be observed for CAT-III (50 wt% Ru–C) and CAT-IV (60 wt% Ru–C). It is worth noting that the intensity of the additional peak is greater in the case of CAT-III than for CAT-IV. It is apparent that the moderate acid sites on the composite samples increases with the increase of Ru–C wt% and the appearance of the new peak indicates the development of relatively strong acid sites in the CAT-III and CAT-IV composite samples.

The CO₂-TPD patterns of the materials are presented in Fig. 3b. A small desorption peak centered at 110 °C can be observed for the CAT-V sample, which can be attributed to physically adsorbed CO₂. In other hand, CAT-I (*n*-ZnO) showed a large desorption peak centered at 290 °C along with the small peak at 110 °C. The peak at 290 °C can be attributed to weak basic sites. All the composite samples showed similar CO₂ desorption patterns as *n*-ZnO. The peak shift to lower energy in CO₂-TPD patterns of composite catalysts indicates that these catalysts possessed relatively weak basic sites than the pure ZnO. An additional desorption peak at 350 °C appeared in all the composite samples and the intensity of this peak is in the order of CAT-III > CAT-IV > CAT-II. It can be seen that the strength of the base sites of the composite samples is not dependent on either Ru–C or *n*-ZnO content. The prepared composite samples show a similar CO₂-TPD pattern as *n*-ZnO, but a larger proportion of moderate and strong base sites are found in the prepared composite samples (in particular CAT-III and CAT-IV). Relatively stronger acid and base sites are observed in CAT-III (50 % Ru–C and 50 % *n*-ZnO), which indicates that an optimum ratio of oxides may be needed to generate the acid and base sites.

Li et al. [30] reported that Ru–ZnO catalysts showed NH₃-desorption peaks in temperature ranges of 150–240 °C (specifically at 170 °C) and 250–425 °C (specifically at 400 °C). The authors also observed that with more Ru content, the position of high temperature peak shifts to lower temperature. This is an indication of lowering of strength of surface acid sites with high Ru content. It was also observed that when the catalyst contained 5 % of Ru, the intensity of NH₃ desorption peak at low temperature increased significantly. The authors also claimed that the extra surface acidity of the catalysts could be due to the generation of new Ru species, which are not reduced to the metal state Ru completely, i.e. Ruⁿ⁺ species in the catalyst. In addition, Yasumoto [31] reported that there is a wide temperature range 100–350 °C for chemisorbed NH₃ and CO₂; the temperature shifts to a lower range, corresponding to the 'q_a' values of 80 and 60 kJ/mol for NH₃ and CO₂ respectively. The observation made by Yasumoto clearly indicating that NH₃ and CO₂ can be adsorbed on ZnO surface relatively at low temperature. In our opinion, a similar phenomenon is happening in case of calcined Ru–C–ZnO composites and showing low

temperature desorption peaks due to presence of finely dispersed ruthenium oxide species.

The distribution of the acidic and basic sites for each of the samples is quite different. The quantities of NH₃ and CO₂ desorbed per gram of catalyst and acid/base site concentration values are summarized in Table 2. The amounts of CO₂ desorbed were estimated by integrating areas under the peaks centered at 280 and 350 °C. The concentration of the acidic and basic sites is measured from the amount of NH₃ and CO₂ desorbed, respectively. The composite catalyst (CAT-III) has the largest concentration of acidic and basic sites when compared to the other composite catalysts; and this may be due to an optimum ratio of *n*-ZnO and Ru–C composition in the sample. However, the acidic/basic site concentration is the highest for the CAT-V sample, which is thought to be due to the acidic functional groups present on the surface of activated charcoal. The addition of *n*-ZnO to Ru–C resulted in an increase in the basic site concentration of the catalysts.

3.6 Self-Condensation of Acetone

It is known that some side reactions during the synthesis of MIBK from acetone do occur (Scheme 1). Besides the aldol condensation of acetone to form DA, acetone can be also hydrogenated over metallic sites to form isopropyl alcohol (IPA). The selectivity towards IPA decreases enormously with increasing temperature because of the exothermic nature of the hydrogenation process of acetone to IPA ($\Delta H = -54.4$ kJ/mol) [20]. The conversion of acetone and selectivity for MIBK over all the catalysts at different reaction temperatures are shown in Fig. 4a, b respectively. As the reaction temperature was increased from 250 to 375 °C, a decrease in the conversion of acetone was observed for all the catalysts. All the composite catalysts showed better conversion than *n*-ZnO or Ru–C alone. The Ru–C catalyst produced 20 % conversion, while *n*-ZnO only showed 10 %. The composite CAT-III showed the maximum conversion of 47 % at 250 °C. The selectivity for MIBK followed a different trend; an increase in the temperature from 250 to 350 °C also resulted in an enhanced selectivity for MIBK but increasing the temperature further to 375 °C caused a decrease in selectivity. We repeated the first set points of catalytic test series at the end of each run and observed a decrease of acetone conversion by 5–8 %. The decrease of catalytic activity is probably due to formation of the water in the reaction of acetone condensation, which negatively influences the metallic centers catalytic activity. These results were in accordance with the results reported in the literature [8].

It is interesting to note that all the catalysts offered the high selectivity to MIBK at 350 °C. The *n*-ZnO again offered less selectivity to MIBK (highest 13 %) than Ru–C

Table 2 TPD of NH₃, CO₂ and catalytic activity results of all the investigated catalysts

Catalyst ^a	CO ₂ ads. (mmol g ⁻¹) ^b	NH ₃ ads. (mmol g ⁻¹) ^b	Acidic/basic site ratio	Conversion of acetone (%)	Selectivity (%)				
					MIBK	IPA	MO	DIBK	Others
CAT-I	0.37	0.03	0.08	5	8	22	45	8	17
CAT-II	0.40	0.23	0.57	9	60	10	3	12	15
CAT-III	0.45	0.46	1.02	30	70	3	2	15	10
CAT-IV	0.41	0.33	0.80	24	54	13	3	18	12
CAT-V	0.04	0.21	5.25	9	15	59	6	10	10

^a Calcined at 400 °C for 12 h in air

^b Catalysts pre-treated in helium gas at 150 °C for 2 h

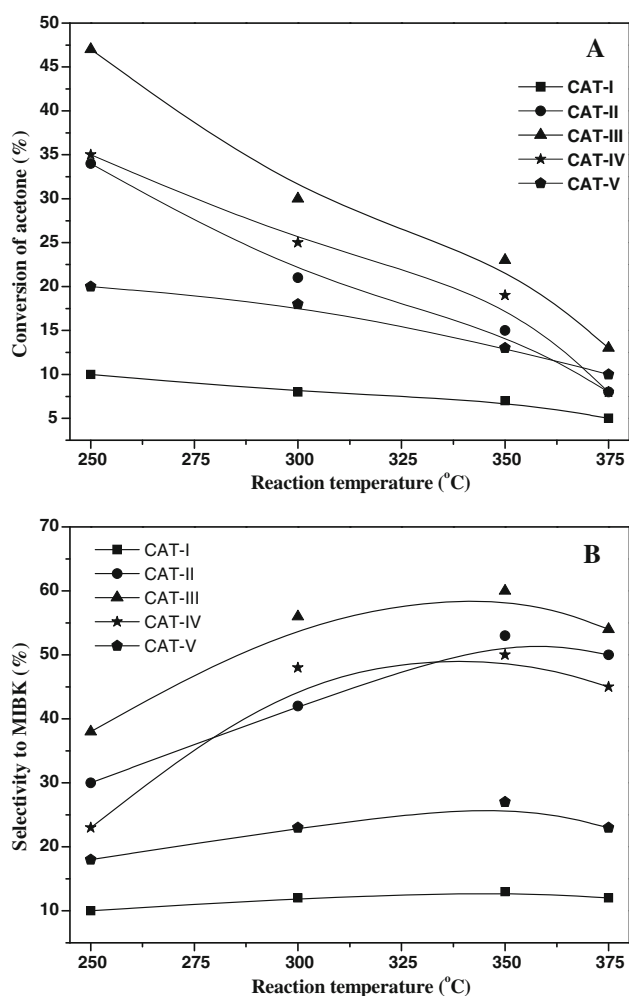


Fig. 4 Catalytic activity of all the investigated catalysts at different reaction temperatures **a** conversion of acetone, **b** selectivity to MIBK; catalyst amount: 250 mg, H₂/acetone molar ratio: 4.5, GHSV: 3,600 h⁻¹

(highest 28 %) at all the reaction temperatures. Di-isobutyl ketone (DIBK), isopropyl alcohol (IPA) and mesityloxyde (MO) are the major products found alongside MIBK. We also found small amounts of DA, mesitylene, propane and propene when all the catalysts were used. The composite catalysts offered better selectivity to MIBK than the pure

oxides and again CAT-III offered the maximum MIBK selectivity of 60 % at 350 °C. Bombos et al. [32] studied the influence of ZnO incorporation to the Pd/H-ZSM-5 catalyst for the synthesis of MIBK. The authors reported that the addition of ZnO caused a decrease in the activity and selectivity for MIBK and concluded that the decrease of acidic centers of the total catalyst was the reason for such behavior.

The TPD results also indicate that Ru-C catalyst have more acidic sites than the *n*-ZnO. The high acidity and activity of Ru-C compared to *n*-ZnO could be due to the presence of surface acid functional groups on the activated carbon [17]. The superior conversion and selectivity of composite catalysts could be linked to synergistic effect between Ru-ZnO and enhancement in acidic and basic functionality of these catalysts. The maximum conversion was attained at 250 °C, whilst the maximum selectivity for MIBK was reached at 350 °C. The selectivity towards IPA decreases upon increasing the reaction temperature for all the catalysts. The condensation and dehydrogenation products catalyzed by acidic sites are favored above 250 °C, while direct hydrogenation products are favored below this temperature (data not presented). It was reported in the literature that metal oxide based catalysts promote the self condensation of acetone by both acid- and base- catalyzed mechanisms [8–10], however deactivation rate would be closely related to the surface basic properties. It was also observed that activity declines due to blockage of both acid and base active sites by a carbonaceous residue formed by secondary reactions. The observations from the literature and our experimental results indicating that balanced acid–base sites, low crystallite size (resistant to coke deposition) are the responsible factors for the observed catalytic activity.

The effect of variation of H₂/acetone molar ratios on acetone conversions and MIBK selectivity at 350 °C are shown in Fig. 5a and b respectively. The conversion increased with increasing H₂/acetone up to a molar ratio equal to 4.5 for all the catalysts. A decrease of conversion of acetone was observed with an increase of H₂/acetone molar ratio from 4.5 to 6. The selectivity towards MIBK formation followed a very similar trend as conversion.

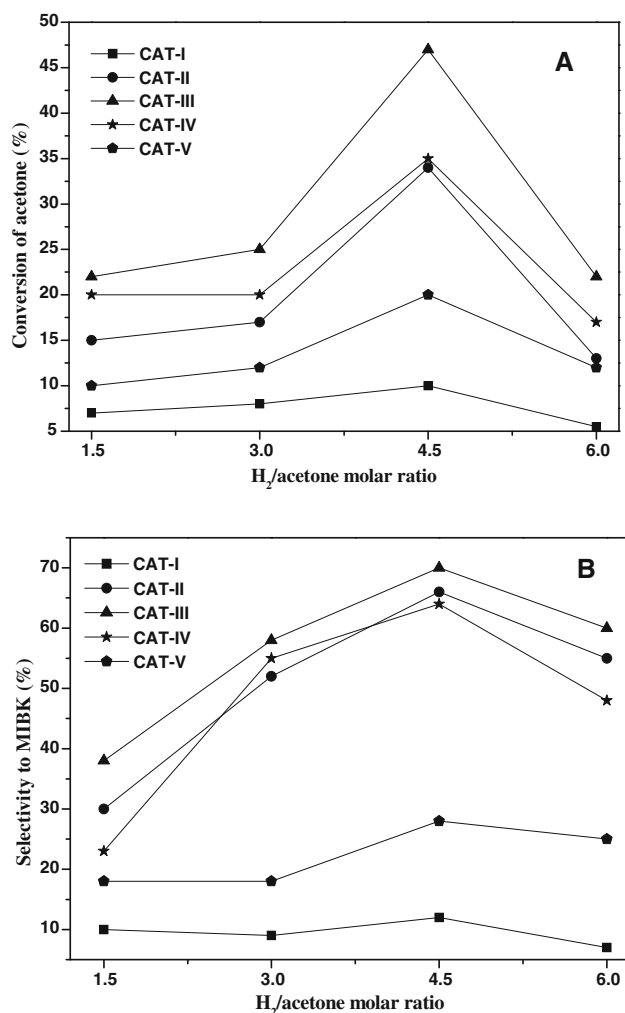


Fig. 5 Effect of H₂/acetone molar ratio on the catalytic performance of the catalysts. **a** Conversion of acetone, **b** selectivity to MIBK. Catalyst amount: 250 mg, reaction temperature: 350 °C, GHSV: 3,600 h⁻¹

CAT-III showed the highest selectivity towards MIBK at a H₂/acetone molar ratio of 4.5. Kozhevnikova et al. [10] observed similar behavior in the case of Pd supported on Zn-Cr mixed oxide catalysts. Thus, a reaction temperature at 350 °C and a H₂/acetone molar ratio of 4.5 were selected as the optimum conditions for MIBK formation selectivity over the CAT-III catalyst.

The conversion of acetone and selectivity for MIBK as a function of Ru-loading is presented in Table 2. Both the conversion of acetone and MIBK selectivity increased with increasing the Ru loading up to 2.5, further increase of Ru loading caused a decrease in conversion and selectivity. The pronounced increase in MIBK selectivity is attributed to the presence of balanced acidic/basic bi-functional sites (hydrogenation and condensation) and optimum crystallite size. Increasing Ru loading above 2.5 wt% resulted in an increase in IPA selectivity, indicating that the high Ru loading favors the

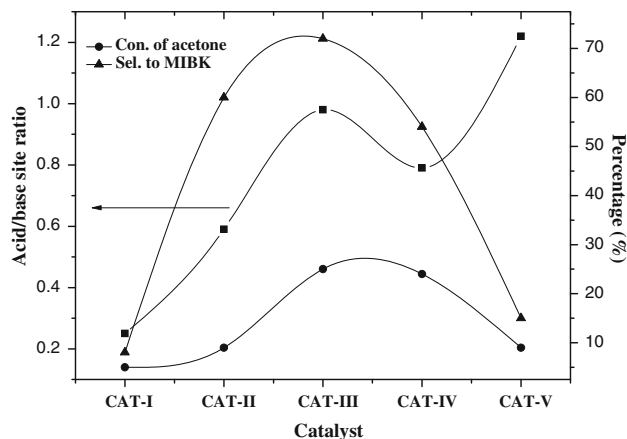


Fig. 6 Correlation between acid/base site ratio and catalytic performance of the catalysts

direct hydrogenation of the acetone carbonyl group. The multifunctional composite catalyst with Ru/C:*n*-ZnO ratio of 1:1 (wt/wt) (CAT-III) exhibited the highest MIBK selectivity. Many literature reports suggest that the formation of MIBK requires the cooperation between metallic and acidic or basic sites, but the hydrogenation of acetone only needs metallic sites [10]. Figure 6 shows the comparison between CAT-I, CAT-II, CAT-III, CAT-IV and CAT-V, and the effect of their acidic/basic site ratio on the acetone conversion and MIBK selectivity at optimum reaction conditions. A direct correlation can be observed for all the catalysts except CAT-V. The activity and selectivity increases steadily with increasing acidic/basic site ratio. CAT-III showed the highest acetone conversion and MIBK selectivity. The high acidic/basic site ratio for CAT-V is due to the acidic functional groups presented on the surface of the AC, but just acidity alone does not play a vital role in the acetone self-condensation reaction. These results showed that the higher activity, the more condensation products were obtained with catalysts that have a balance of acid/base sites.

It is reported that any catalyst that contains a metal-metal oxide interface, where electron-deficient sites such as oxygen vacancies exist in close proximity to metallic hydrogenating sites, can perform better in the self-condensation reaction of acetone [11]. This metal-metal oxide interface can be created either by a partially reduced metal oxide or as a consequence of a metal-support interaction like the formation of a solid solution. It is also known that when an *n*-type semiconductor particle, such as ZnO, is exposed to air, oxygen molecules can be adsorbed onto the surface of the particle and form O₂⁻, O₂²⁻ and O²⁻ ions by capturing electrons from the conduction band, which in turn produces an electron-depleted space charge layer in the surface region of the particle [33]. Even though oxygen is not presented in the reactants, ZnO could still be exposed to oxygen due to in situ formation of H₂O in the

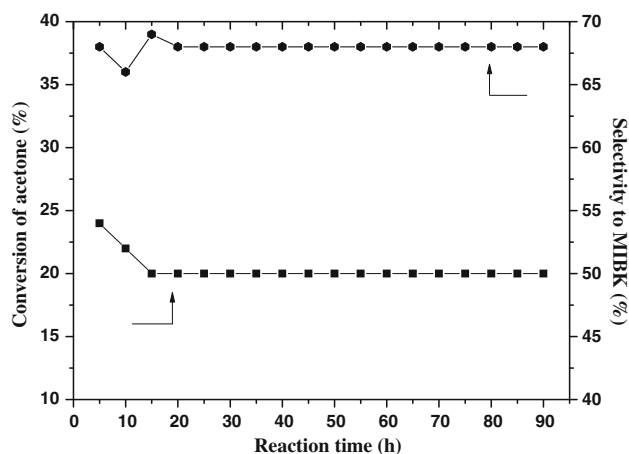


Fig. 7 Time on stream analysis over CAT-III catalyst; catalyst amount: 250 mg, H_2 /acetone molar ratio: 4.5, GHSV: $3,600\text{ h}^{-1}$

condensation reaction. The carbonyl group of acetone could be activated by attachment to the surface of the oxides through coordination of the O-atom to the M^{n+} surface site. The surface O^{2-} ion can act as a basic site to extract a methyl proton resulting in the formation of a nucleophile species [34]. This reacts with a neighboring coordinated carbonyl centre in the presence of adsorbed hydrogen atoms on metallic sites to form a molecule of MIBK and water. It is reported that both the acidic and basic sites of the catalysts are involved in the aldol condensation step [35]. In other words; formation of products like MIBK, MO or DIBK is controlled by the acidic/basic bi-functional nature of the catalysts.

Time-on-stream studies with the composite catalysts show no appreciable loss in activity for a period of 100 h. Figure 7 shows the conversion of acetone and selectivity for MIBK response for our best-performing catalyst (CAT-III). The catalyst reaches a steady state in approximately 1 h and the conversion and MIBK selectivity are maintained constant for 100 h. These results indicate the suitability of a Ru-C-ZnO catalyst for industrial application for the acetone condensation process.

4 Conclusions

The Ru-C-n-ZnO composite catalysts are efficient for the synthesis of MIBK by reductive condensation of acetone in the gas phase. The best MIBK selectivity from one step, acetone self-condensation over Ru-C-n-ZnO was obtained at $350\text{ }^\circ\text{C}$, H_2 /acetone = 4.5 and Ru loading = 2.5%. A catalyst with Ru-C:n-ZnO ratio is 1:1 (wt%/wt%) showed the highest acetone conversion and

selectivity to MIBK. Time-on-stream analysis also showed that this catalyst offers good durability for the gas-phase, one-step synthesis of MIBK. TEM analysis of the composite catalysts provided the information that a synergistic effect existed between Ru-ZnO and TPD results indicated the enhancement in acidic and basic centers in these catalysts. Superior performance of the CAT-III composite catalyst could be directly linked to its balanced hydrogenation and acid-base functional character.

Acknowledgments The authors are grateful to Felicity Sartain, Bio-Nano Ltd., UK for her support in revising English, W. Schwieger, Alexandra Inyat, Amer Inyat, Hallah Alyousef, Dirk Enk, University of Erlangen-Nuernberg, Germany for their technical support in catalyst characterization, Abdulaziz AL-Ghashem, Muhamad Ashinqiti, Muhamad Ashammeri and Faez Al-Otaibi, King Abdulaziz City for Science and Technology (KACST) for their support in reactor operation. KACST is acknowledged for funding this work under project No. 29-280.

References

- Zhang G, Hattori H, Tanabe K (1988) *Appl Catal* 36:189
- Reichle WT (1980) *J Catal* 63:295
- Zahn H, Krasowski A (2002) *Ullmann's encyclopedia of industrial chemistry*, 6th edn (CD ROM). Wiley-VCH, Weinheim
- Reith W, Dettmer M, Widdecke H, Fleischer B (1991) *Stud Surf Sci Catal* 59:487
- Weissermel K, Arpe HJ (1997) *Industrial organic chemistry*. Wiley, Germany
- Lawson KH, Nkosi B (1999) US Patent 6,008,416
- Mitschker A, Wagner R, Lange PM (1988) In: Guisnet M (ed) *Heterogeneous catalysis and fine chemicals I*. Elsevier, Amsterdam
- Talwalkar S, Mahajani S (2006) *Appl Catal A* 302:140
- Yang SM, Wu YM (2000) *Appl Catal A* 192:211
- Kozhevnikova EF, Kozhevnikov IV (2006) *J Catal* 238:286
- Martinez-Ortiz MJ, Tichit D, Gonzalez P, Coq B (2003) *J Mol Catal A* 201:199
- Unnikrishnan R, Narayanan S (1999) *J Mol Catal A* 144:173
- Unnikrishnan R, Narayanan S (1996) *Appl Catal A* 145:231
- Chikan V, Molnar A, Balazsik K (1999) *J Catal* 184:134
- Molnar A, Varga M, Mulas G, Mohai M, Bertoti I, Lovas A, Cocco G (2001) *Mater Sci Eng A* 304–306:1078
- Hetterley RD, Kozhevnikova EF, Kozhevnikov IV (2006) *Chem Commun* 7:782
- Waters G, Richter O, Czarnetzki BK (2006) *Ind Eng Chem Res* 45:6111
- Bagabas AA, Akhmedov V, Mostafa MM, Al-Rabiah A (2011) US Patent 7,951,976, 31 May 2011
- Galvagno S, Capannelli G (1991) *J Mol Catal* 64:237
- Tanabe K, Shimazu K, Hattori H, Shimazu K (1979) *J Catal* 57:35
- Bagabas AA, Apblett A, Shemsi A, Seddigi Z (2008) *Main Group Chem* 7:65
- Navale SC, Ravi V, Mulla IS (2009) *Sens Actuators B* 139:466
- Hosono E, Fujihara S, Kimura T, Imai H (2004) *J Sol-Gel Sci Tech* 29:71
- Baeza BB, Ruiz AG, Ramos IR (2000) *Appl Catal A* 192:289
- Baeza BB, Ruiz AG, Wang P, Ramos IR (2001) *J Catal* 204:450

26. Wang JQ, Wang YZ, Zhe SH, Qiao MH, Li HX, Fan KN (2004) *Appl Catal A* 272:29
27. Neri G, Mercadante L, Donato A, Visco AM, Galvagno S (1994) *Catal Lett* 29:379
28. Fernandez EVR, Ferreira AFP, Escribano AS, Kapteijn F, Reinoso FR (2008) *J Catal* 258:52
29. Wiberg KB, Crocker LS, Morgan KM (1991) *J Am Chem Soc* 113:3447
30. Li B, Hu G-S, Jin L-Y, Hong X, Lu J-Q, Luo M-F (2013) *J Ind Eng Chem* 19:250
31. Yasumoto I (1984) *J Phys Chem* 88:4041
32. Bombos D, Bozga G, Bombos M, Stefan A, Stanciu I (2000) *Chem Pap* 54:171
33. Morrison SR (1987) *Sens Actuators B* 12:425
34. Idriss H, Kim KS, Barteau MA (1993) *J Catal* 139:119
35. Di Cosimo JJ, Diez VK, Apesteguía CR (1996) *Appl Catal A* 137:149